minerals

MDPI

Article

Mineralogical Analysis of the Kestel Mine: An Early Bronze Age Source of Tin Ore in the Taurus Mountains, Turkey

Wayne Powell [1,*], Evren Yazgan [2], Michael Johnson [3], K. Aslıhan Yener [4] and Ryan Mathur [5]

[1] Department of Earth and Environmental Science, Brooklyn College, Brooklyn, NY 11210, USA
[2] General Directorate of Mineral Research and Exploration (MTA), Ankara 06530, Turkey; evren.yazgan43@gmail.com
[3] Stell Environmental Enterprises, Eagleview Corporate Center, Exton, PA 19341, USA; mjohnson086@gmail.com
[4] Institute for the Study of the Ancient World (ISAW), New York University, New York, NY 10028, USA; akyener12@gmail.com
[5] Department of Geology, Juniata College, Huntingdon, PA 16652, USA; MATHURR@juniata.edu
* Correspondence: wpowell@brooklyn.cuny.edu

Abstract: Since its discovery in 1987, the Early Bronze Kestel Mine has been a topic of archaeological and geological controversy. The initial interpretation of the extensive marble-hosted galleries as the oldest known tin mine was challenged due to the low tin grade in remaining hematite-quartz veins, and it was suggested that Kestel was more likely mined for gold. Mineralogical analysis of the remaining mineralization was compared to a heavy mineral concentrate extracted from the soil preserved within the mine. The compositionally complex, arsenate-rich mineral assemblage from the mine sediment, contrasts with that of the remaining surface mineralization. Thus, the outcropping veins do not represent the nature of the extracted ore. Only one grain of gold was found in the heavy mineral concentrate, whereas cassiterite composed 1.5% of the sample. Cassiterite occurs in complex assemblages with arsenates, clays, hematite, quartz, and dolomite, bearing resemblance to hematite-arsenate tin mineralization that occurs near Kayseri, 60 km to the northeast. These findings indicate that although gold was a trace component of the Kestel ore, cassiterite was the mineral of interest to the Early Bronze Age miners, and that Kestel represents the earliest evidence thus far for an emerging pattern of local tin exploitation.

Keywords: geoarchaeology; Bronze Age; cassiterite; arsenates; Turkey; Niğde Massif

Citation: Powell, W.; Yazgan, E.; Johnson, M.; Yener, K.A.; Mathur, R. Mineralogical Analysis of the Kestel Mine: An Early Bronze Age Source of Tin Ore in the Taurus Mountains, Turkey. *Minerals* **2021**, *11*, 91. https://doi.org/10.3390/min11010091

Received: 30 December 2020
Accepted: 15 January 2021
Published: 19 January 2021

1. Introduction

Archaeologists continue to seek to identify the sources of tin ore that supplied the extensive bronze production of the eastern Mediterranean during the Bronze Age. Given that the region lacks major cassiterite deposits, researchers have focused on distant sources such as the English deposits of Cornwall, the Bohemian ores of the Erzgebirge, and mines of Central Asia (Tajikistan, Afghanistan, Pakistan) [1–4]. An early second-millennium BC cuneiform tablet excavated from the Central Anatolian trading center of Kültepe describes tin being brought to the city of Assur in northern Iraq from an unknown location in the east, and then transported to Turkey by donkey caravans, consistent with a Central Asian origin of the metal [1]. However, tin bronzes existed 1000 years before the abovementioned texts during the Late Chalcolithic/Early Bronze Age. Others have concluded that a single source model is untenable, and that smaller tin deposits that would be considered subeconomic by modern standards likely contributed significantly to the prehistoric metal economy [5–8].

The ancient mining site of Kestel in the Central Taurus Mountains of Turkey (35 km southeast of the city of Niğde; Figures 1 and 2) presents the most compelling archaeological evidence for early tin production proximal to the Eastern Mediterranean. Following the General Directorate of Mineral Research and Exploration's discovery of placer cassiterite

in the Kuruçay stream, near the town of Celaller (Figure 1), open pit mines and collapsed gallery entrances were discovered over 2 km^2 on the adjacent hillside [5]. To date, archaeologists have documented 1.5 km of underground workings totaling more than 4500 m^3 of galleries at the Kestel mine [9]. Ore was mined predominantly from a marble host, but also from quartzite and pegmatite dikes [9]. Open pit workings were first exploited at the beginning of the Early Bronze Age, around 3000 BC [10]. Ceramic typology and carbon dating of charcoal from within the mine indicate that construction of the underground shaft and gallery network was begun shortly after, and that mineral processing at the site reached its height towards the end of the Early Bronze Age (ca. 2000 BC) [10].

Hematite-quartz veins in the wall of the mine chambers were found to contain up to 7900 ppm Sn and approximately 0.5 g/ton gold; both native gold and cassiterite were found in veins and soils within the mine [11]. Pieces of hematite vein materials with low tin content were discarded in the mine and downslope, and Sn-barren hematite veins remain unmined. Furthermore, Earl and Özbal [11] noted that hematite lumps that were excavated from the ore processing site of Göltepe, 2 km southeast of the Kestel mine, contained three times the average Sn concentration of vein material from Kestel, 647 and 2080 ppm respectively; powdered hematitic ore found in ceramic containers at the same site were even more enriched, with 4464 ppm tin, suggesting that ore was being treated to concentrate tin [11]. In addition, over one ton of ceramic crucible fragments were excavated from Göltepe [10]. Vitrified surfaces on the inner surfaces of these fragments contain up to 4% tin [9]. Based on these findings, the archaeological team led by K.A. Yener concluded that Kestel was worked for its tin ore.

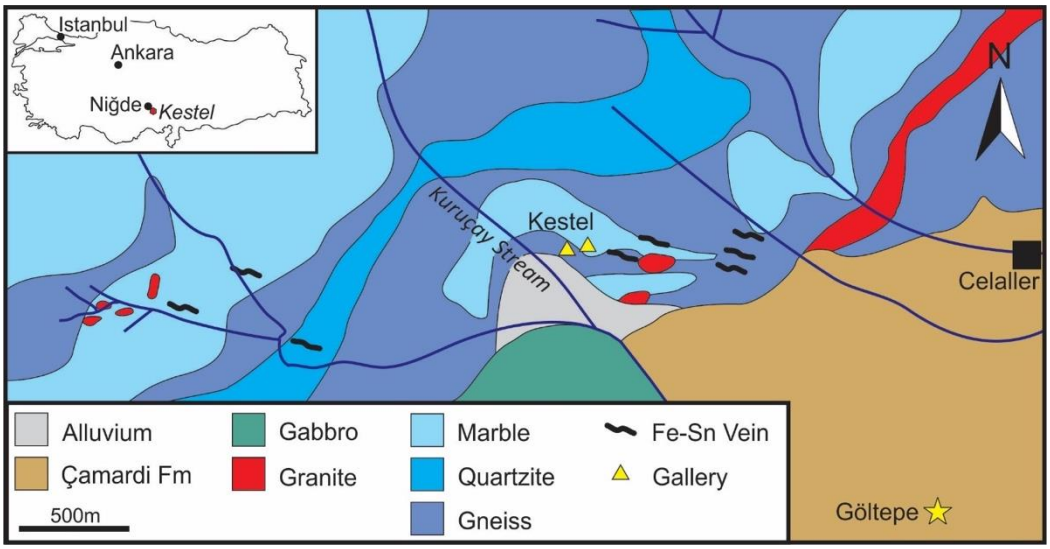

Figure 1. Local geology of the Kestel Mine [12].

1.1. The Controversy

Publication of the initial findings at Kestel initiated a heated debate in the archaeological literature as to the veracity of Yener's conclusions. Muhly [13] conducted his own petrographic analysis of a sample taken from an unmined vein above the Kestel mine entrance. He observed no cassiterite in polished section, and only trace cassiterite in the heavy mineral fraction, indicating a total Sn content of only 26ppm. However, the sample contained several 50µ grains of native gold, leading Muhly [13] to suggest that Kestel was a ferruginous gold deposit, and that gold was the mined commodity, not tin.

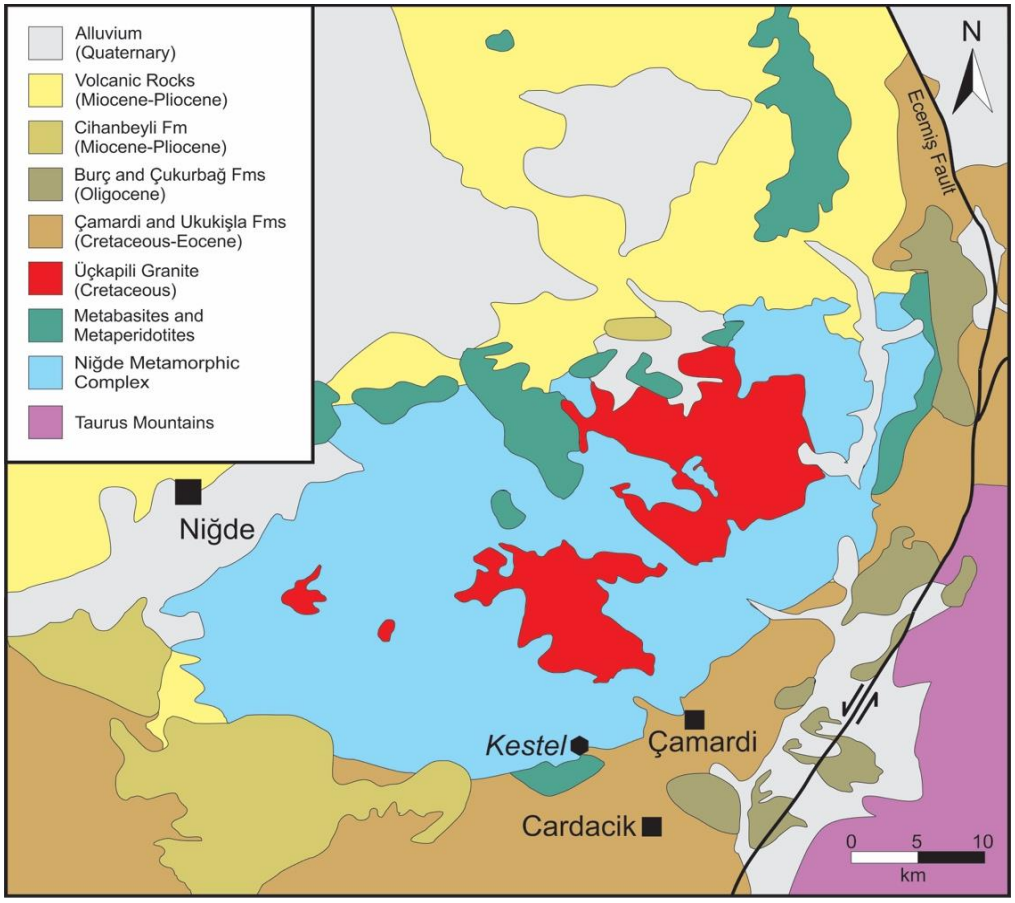

Figure 2. Geology of the Niğde Massif and surrounding area [14].

A similar argument was voiced by Hall and Steadman [15], who referred to cassiterite as a trace mineral at Kestel, as well as by Pernicka et al. [16] (p. 95) who described cassiterite at the site to be "mineralogically very interesting, but economically marginal". Ultimately Muhly et al. [13,17], Steadman and Hall [15], and Pernicka et al. [16] agreed that it is not self-evident that Kestel had been a tin mine, and more likely is the remnants of a gold deposit. Iron oxide copper gold ores (IOCG) are widely distributed across Turkey [18–20], and an unpublished mining exploration map included in Muhly [13] identify seven occurrences of gold in the immediate vicinity of Kestel. Thus, the true nature of the ore has remained uncertain.

A mine is abandoned only when ore can no longer be extracted profitably due to either a decrease in the value of the commodity, or the exhaustion of all economically viable mineralization. Both tin and gold maintained their value for millennia. Therefore, it is reasonable to conclude that the ore at Kestel was exhausted, and that the presently observed mineral assemblages and metal concentrations characterize waste rather than ore. Therein lies the problem in interpreting the nature of the Kestel mine. As stated by Hall and Steadman [15] (p. 218) "tin could have existed in higher concentrations and been mined to its present levels through time, but speculation on this matter is fruitless until more geological and archaeological data are presented".

Whether tin or gold had been the metal of interest, it seems assured that the original ore grade will remain a mystery. However, insights into the nature of the ore and the commodity of interest may be recorded in the fine detrital mineral grains that were derived from the mining and crushing of the ore and are preserved in the soils both within and downslope of the mine [5,11].

Archaeological surface survey identified ore dressing sites mainly located near mine openings, including one on the roof of the main chamber of the Kestel mine immediately

above the entrance [21]. The marble platform has 216 circular mortar-like depressions (Figure 3) that are interpreted to have been used for ore crushing. They range in size from 5–9 cm in diameter and with depths of 1–4 cm [21]. Based on the topography of the immediate area, material from this ledge would wash toward the mine entrance, which then slopes inward. Thus, during the mining and ore dressing activities traces of the fine-grained, crushed ore would have accumulated in the soils/sediments within the Kestel chambers, thereby preserving a record of the mineralogical composition of the extracted ore. This paper documents the ore minerals contained in soils at the mouth and just within the entry chamber of the Kestel mine and compares this assemblage to that of remnant hematite-quartz vein mineralization in order to further characterize the Kestel deposit.

Figure 3. Ore crushing pits in marble platform above entrance of Kestel mine.

1.2. Regional and Local Geology

The Niğde Massif (Figure 2) of the Central Anatolian Crystalline Complex is a migmatite-cored structural dome that was exhumed in the Late Cretaceous [14]. The high-grade metamorphic core of the western belt is composed of metapelitic rocks and calc-silicate rocks, marble, and amphibolite of the Gümüşler Formation [14]. The Eastern Belt, in which the Kestel mine is located, is a lower-grade marble-dominated sequence that is more extensively overprinted by late brittle faulting [14]. The Gümüşler Formation is intruded by the Late Cretaceous (85–92 Ma) Üçkapılı granitoid [22] (Figure 2). This pluton is composed of peraluminous granites and granodiorites derived from crustal melting, as well as tholeiitic mafic enclaves derived from a subduction-modified mantle source [23]. These researchers interpret the Üçkapılı granitoid as having formed as a result of post-collisional magmatism associated with lithospheric delamination and mafic magma underplating. Rapid emplacement of the granite to <10 km depth occurred during extensional exhumation of the Niğde Massif [14].

Regionally, mineralization is spatially and genetically associated with Üçkapılı intrusive rocks. This includes Fe-skarns [24], and vein-deposits of Fe [25] and Sb-Hg [26]. The Madsen Sb-Hg deposit, 1 km north-northeast of Çamardı (Figure 2), consists of quartz-stibnite ± pyrite veins along foliation planes, fold crests, and marble-gneiss contacts in the Gümüşler Formation, and is associated with silicification, sericitization, and chloritization [26]. Iron mineralization is irregularly distributed throughout the supracrustal unit of the Niğde Massif in the form of lenses, breccias, and veins composed predominantly of hematite [26]. Tumuklu et al. [25] also notes the presence of lesser goethite-limonite, magnetite, and copper minerals (mainly chalcopyrite, with secondary malachite, native copper, covellite, and chalcocite) comprise <1% of the ore; trace gold is also present; kaolinitization accompanies Fe mineralization.

The mineralization currently exposed at Kestel exhibits similarities to the iron deposits of the region. East-west-striking hematite quartz veins and quartz-tourmaline veins up to several centimeters thick cut marble, gneiss, and kaolinized and sericitized Üçkapılı-type granitic rocks [27] (Figure 1). Tin grade in these veins varies between 0.15 and 0.6 wt% and cassiterite crystals are <0.8 mm [27]. Carbonate minerals (calcite, dolomite, siderite, ankerite) are the only other abundant minerals within these veins. Trace amounts of pyrite, native bismuth, arsenopyrite, pyrrhotite, and native gold were observed; primary chalcocite has been replaced by covellite and malachite, and arsenopyrite is partially replaced by scorodite [27].

2. Materials and Methods

In order to characterize the residual (waste) mineralization in the field, the composition of in situ hematite-quartz veins and loose hematite vein material were analyzed in the field with an Olympus Innov-X Delta Classic DC-4000 (with 3-Beam Soil software) portable X-ray fluorescence (pXRF) hand-held apparatus. Three cobble-sized samples of this rock were collected from the hillside downslope of the Kestel mine to further characterize the residual (waste) mineralization. Polished thin sections were produced for analysis. Reconnaissance x-ray mapping of Fe, Cu, As, Sb, W, Sn, Au, Pb, and Bi was conducted across the polished sections to identify phases of interest. X-ray mapping and point analyses for mineral identification and textural characterization were conducted on three polished sections and one rough, unprepared surface on the Hitachi TM3030Plus scanning electron microscope (Brooklyn College, Brooklyn, USA) operating at 15 kV and an Oxford Instruments AZtec energy dispersive spectrometer with the Oxford Instruments AZtecOne software platform.

A bulk soil sample taken from the main chamber near the entrance of the Kestel mine was sieved to remove material greater than 2 mm, and then washed and floated to remove the organic and clay components. The residual sediment was then panned to produce a black sand concentrate. Samples were subsequently dried and the heavy mineral concentrate was further purified by extracting light minerals (<2.9 g/cm^3) using flotation separation with a solution of sodium polytungstate ($3Na_2WO_4 \cdot 9WO_3 \cdot H_2O$), resulting in a 26.5 g sample. The heavy mineral assemblage was then fed through a Frantz Isodynamic Magnetic Separator after magnetite was removed using a hand magnet. Subsamples were taken at 0.4 A, 0.5 A, 0.75 A, 1.0 A, 1.5 A, 2.0 A and the remaining non-magnetic fraction. Each fraction was weighed and mounted on aluminum stubs with carbon tape for analysis.

All heavy mineral grains were identified and characterized using the Hitachi TM3030Plus-Aztec system as described above. Reconnaissance x-ray mapping for heavy metals (Ti, Cr, Mn, Fe, Ni, Cu, Zn, As, Ag, Sn, Sb, Ba, W, Au, Hg, Pb, Bi) was conducted to target analysis and identification of ore suite minerals. Semi-quantitative point analyses were used to define the major element components of mineral grains and determine approximate molar proportions from which mineral formulae/identities were deduced stoichiometrically. Physical features observable under the scanning electron microscope (form, cleavage) and binocular microscope (color, luster) were also noted and used for mineral identification. Point counts were conducted on representative samples of each magnetic fraction to determine the modal composition.

3. Results

3.1. In Situ Veins and Surface Finds

pXRF analysis of the sub-horizonal in situ hematite-quartz veins (Figure 4) was consistent with published results; much of the material was barren, but Sn values of up to 0.5% were recorded. Other than Fe and Sn, no other metals were present at >100 ppm. The 10 cm wide vein that outcrops above the mine entrance (Figure 4A) displays a scar from channel sampling (Figure 4B). It is likely that this is the site of the "trench samples [that] were taken from a mineralized vein in the vicinity of the mine entrance at Kestel" [16] (p. 94) that were taken by Muhly. This sample was reported to contain 26 ppm Sn and trace Au [13]. Tin was below the detection limit of the pXRF (<150 ppm) at the prior sample site

in the vein, consistent with published results [13]. However, the 0.5m length of reddish vein material immediately to the left of the sample site (Figure 4B) contains 0.2–0.5% Sn. pXRF spot analyses of loose hematite-quartz waste rock ranged from undetectable to as high as 4% Sn, with no other metals present at concentrations >150 ppm, aside from iron.

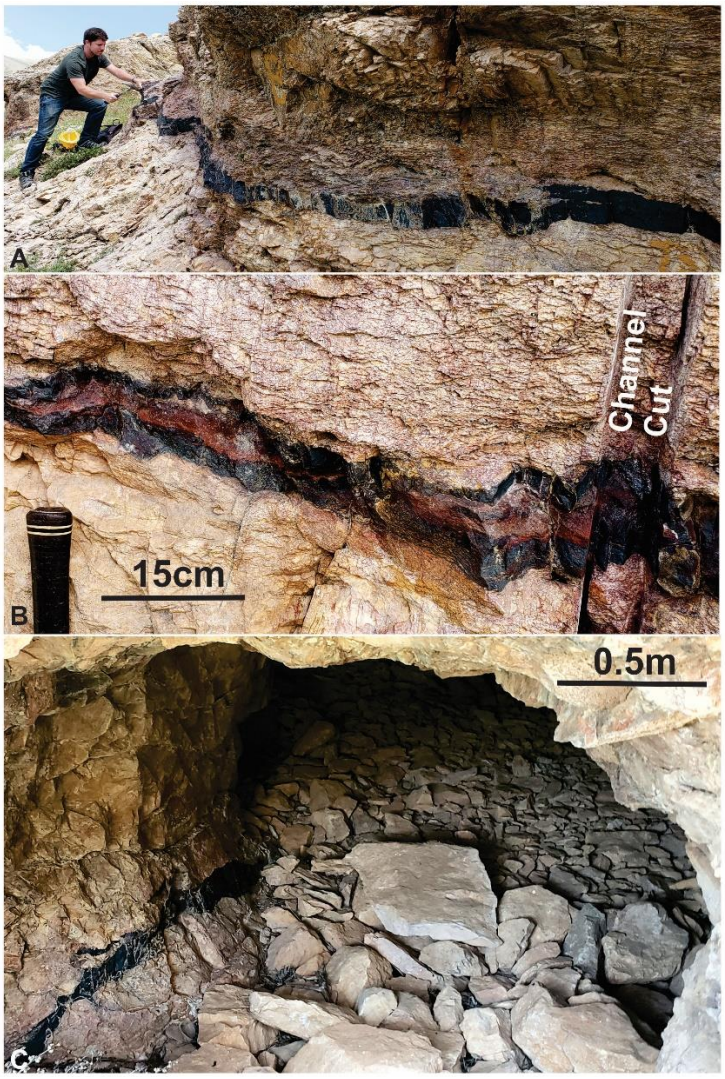

Figure 4. In situ outcroppings of hematite-quartz veins. (**A**) Vein immediately above the main mine entrance; (**B**) close-up of A showing channel sample from prior analysis; (**C**) hematite-quartz vein exposed in wall of collapsed mine entrance.

Petrographic and SEM analysis of the mineralized samples indicate that composition varies. Figure 5 illustrates an example of hematite-quartz matrix with minor tourmaline, as has been described by Çağatay and Pehlivan [27]. In hand-sample, reddish-brown cassiterite can be seen set in a matrix of black hematite and red quartz (Figure 5A). The cassiterite is concentrated in late veinlets and micro-breccias with hematite matrix (Figure 5C–F). These breccias incorporate clasts of older tin-mineralized rock in which cassiterite is hosted by quartz (Figure 5G,H). No additional ore minerals were observed in this sample using both reflected light microscopy and SEM analysis.

Table 1. Minerals identified in heavy mineral separate and hand samples.

Mineral Name	Abbreviation in Text	Formula
Native Antimony	Sb	Sb
Native Bismuth		Bi
Native Gold		Au
Arsenopyrite	Apy	FeAsS
Cinnabar		HgS
Wittechinite		$CuBiS_3$
Hematite	Hem	Fe_2O_3
Magnetite		Fe_3O_4
Ilmenite		$FeTiO_3$
Chromite		$FeCr_2O_4$
Cassiterite	Cst	SnO_2
Rutile		TiO_2
Damaraite		$Pb_3O_2(OH)Cl$
Beyerite	Bey	$Ca(BiO_2)(CO_3)_2$
Calcite	Cal	$CaCO_3$
Cerussite	Cer	$PbCO_3$
Dolomite	Dol	$MgCa(CO_3)_2$
Barstowite	Bst	$Pb_4Cl_6(CO_3) \cdot H_2O$
Barite		$BaSO_4$
Apatite	Ap	$Ca_5(PO_4)_3(F,Cl,OH)$
Monazite	Mnz	$(Ce,La,Nd,Th)PO_4$
As-Monazite	As-Mnz	$(Ce,La,Nd,Th)(As,P)O_4$
Phosphohedyphane		$Ca_2Pb_3(PO_4)_3Cl$
Plumbogummite		$PbAl_3(PO_4)(PO_3OH)(OH)_6$
Fluorcalcioroméite		$(Ca,Na,\square)_2Sb^{5+}{}_2(O,OH)_6F$
Arsenoflorencite		$(Ce,La,Nd)Al_3(AsO_4)_2(OH)_6$
Berzeliite	Brz	$(NaCa_2)Mg_2(AsO_4)_3$
Chernovite		$YAsO_4$
Mimetite		$Pb_5(AsO_4)_3Cl$
Sewardite	Sew	$CaFe^{3+}{}_2(AsO_4)_2(OH)_2$
Hydrotungstite	Htu	$WO_3 \cdot H_2O$
Raspite	Ras	$PbWO_4$
Garnet		$(Fe,Mg,Ca)_3Al_2(SiO_4)_3$
Titanite		$CaTi(SiO_4)O$
Zircon		$ZrSiO_4$
Tourmaline	Tur	$Na(Mg_3)Al_6(Si_6O_{18})(BO_3)_3(OH)_3(OH)$
Diopside		$CaMgSi_2O_6$
Hornblende		$(Ca,Na)_{2–3}(Mg,Fe,Al)_5(Al,Si)_8O_{22}(OH,F)_2$
Chlorite		$(Mg,Fe)_5Al(Si_3Al)O_{10}(OH)_8$
Quartz	Qz	SiO_2

Figure 6 illustrates another form of brecciated mineralization in which clasts of hematite and calcite are set in a matrix of quartz and mixed-layer clays, with minor apatite. Cassiterite occurs as the fill of microbreccias and veinlets within the quartz-clay intergrowths (Figure 6B–D). Trace As-monazite [$(Ce,La,Nd,Th)(As,P)O_4$] occurs in the quartz-clay matrix (Figure 6D,E), and trace native bismuth is present in both quartz-clay matrix and clasts of hematite.

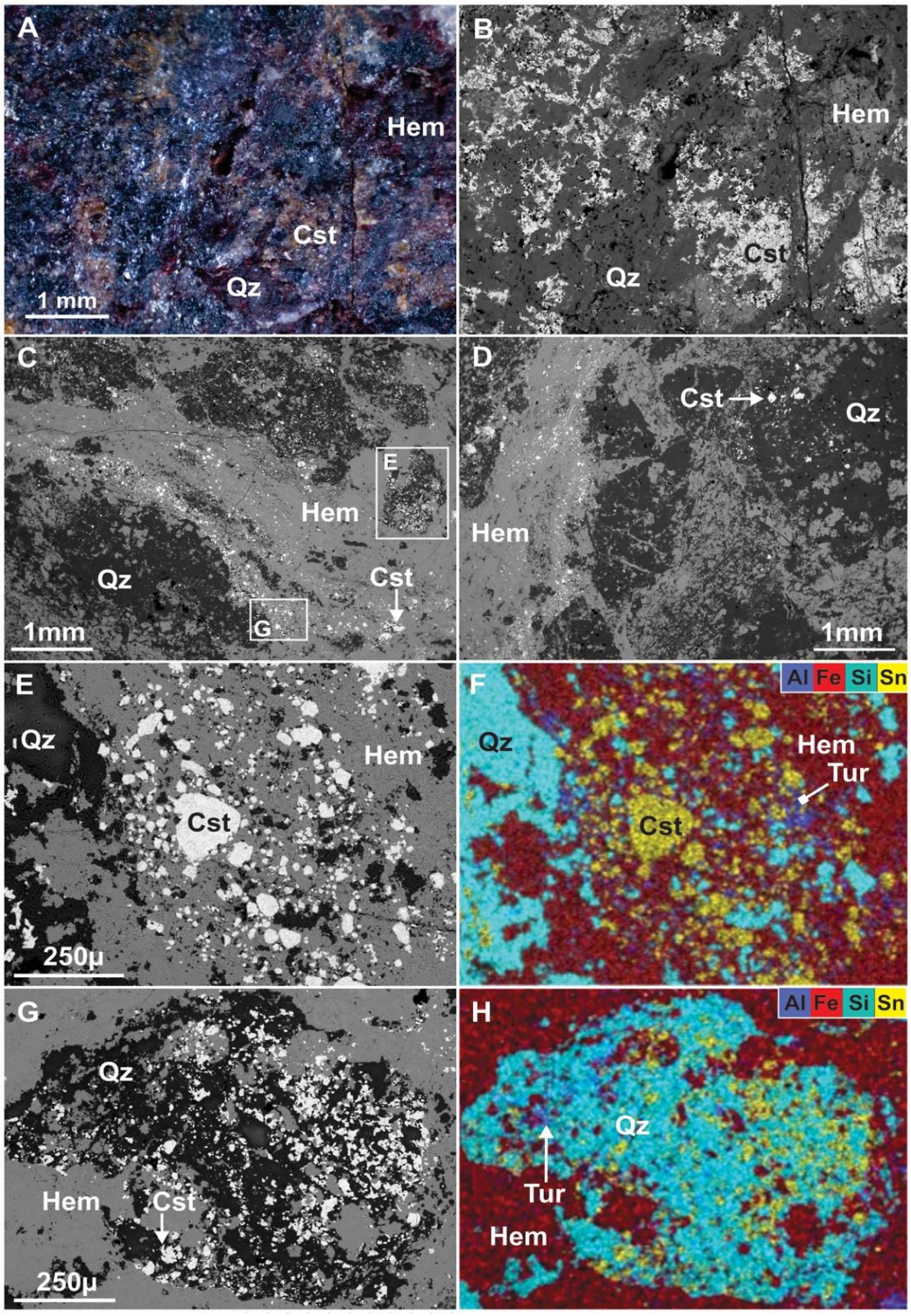

Figure 5. Hematite-Quartz-Cassiterite vein breccia. Mineral abbreviations listed in Table 1. (**A**) Photograph of ore; (**B**) Backscatter electron (BSE) image of (**A**); (**C**) Hem-Cst veinlet cutting quartz-rich breccia; (**D**) quartz clasts in Hem-Cst matrix; (**E**) close-up of Hem-Cst matrix in (**C**); (**F**) BSE image of (**E**); (**F**) close-up of Qz-Cst clast in Hem-Cst in (**C**); (**H**) X-ray map of (**G**). Hem: Hematite; Cst: Cassiterite; Qz: Quartz; Tur: Tourmaline.

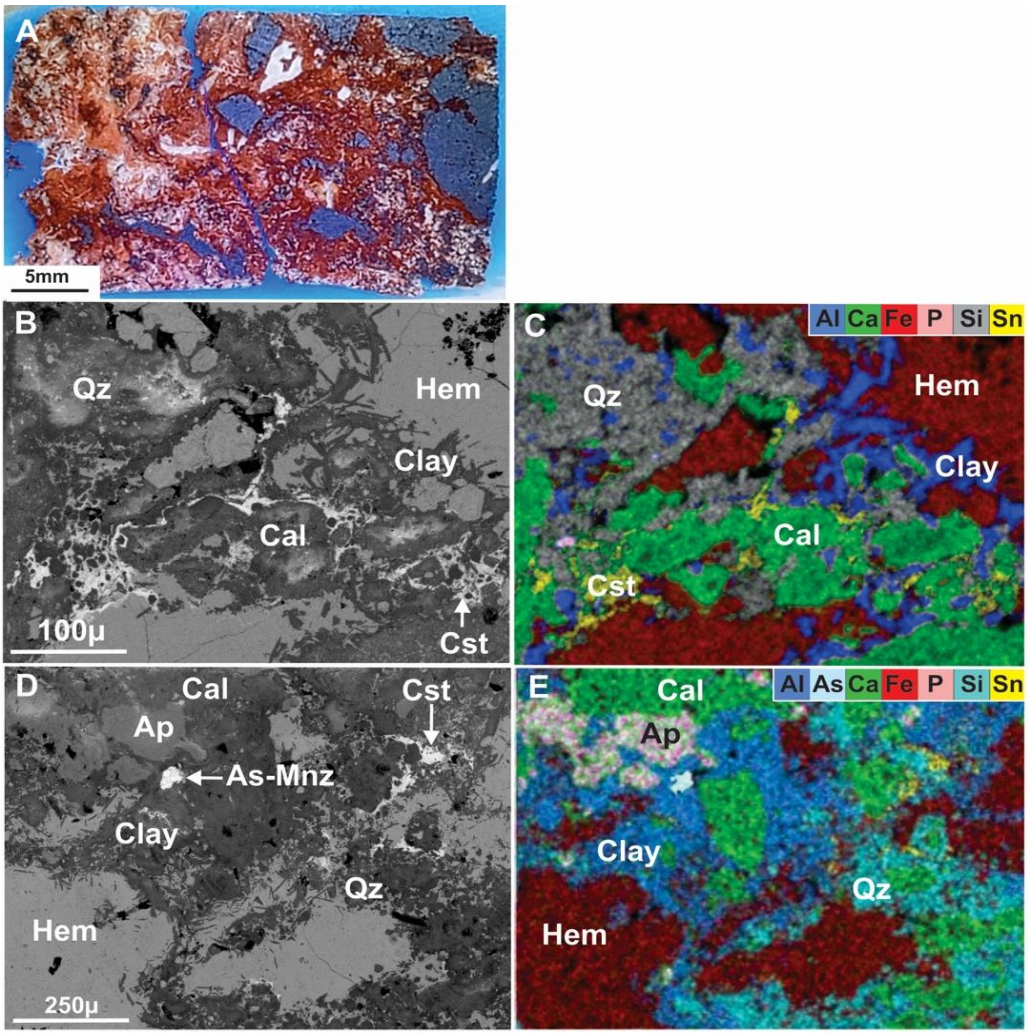

Figure 6. Hematite-Quartz-Calcite vein breccia. (**A**) Photograph of polished thin section; (**B**) Breccia with Cst-bearing clay-rich matrix; (**C**) X-ray map of (**B**); (**D**) Breccia with Cst-bearing clay-rich matrix with apatite and As-monazite; (**E**) X-ray map of (**D**). Cal: Calcite; Ap: Apatite; As-Mnz: As-Monazite.

3.2. Heavy Mineral Concentrate

Hematite and magnetite are the predominant minerals, comprising 61% and 21% of the concentrate, respectively. Ilmenite (5%), tourmaline (2%), diopside (2%), and cassiterite (1.5%) are the only other minerals present at >1% based on point count analysis. The sample contained one grain of gold, 350µ in length.

The complete list of minerals that comprise the heavy mineral fraction is presented in Table 1. In addition to diopside and tourmaline, common silicates included garnet, hornblende, chlorite, titanite, and zircon. Sulfide minerals were rare; arsenopyrite was most abundant; single grains of cinnabar and wittechinite ($CuBiS_3$) were identified. Barite is the only sulfate mineral present.

Arsenates are the most diverse mineral group in the Kestel heavy mineral assemblage. Mimetite ($Pb_5(AsO_4)_3Cl$) is the most abundant and occurs as rounded grains of radiating yellow resinous acicular crystals (Figure 7A). Blocky, subhedral, colorless berzeliite ($(NaCa_2)Mg_2(AsO_4)_3$) (Figure 7B) is rarer, as is deep red, vitreous sewardite ($CaFe^{3+}{}_2(AsO_4)_2(OH)_2$) which occurs in platy and subhedral blocky forms (Figure 7C), as well as within composite grains with cassiterite, hematite, quartz, clay, and dolomite. Two rare earth element-bearing arsenates were documented, arsenoflorencite (Ce,La,Nd)-$Al_3(AsO_4)_2(OH)_6$ (Figure 7D) and chernovite ($YAsO_4$) (Figure 7E). Both occur as euhedral crystals, dipyramidal and scalohohedral, respectively. One subhedral, angular grain of a

Cu-Ca-bearing arsenate was found with micro-veinlets of cassiterite (Figure 7F), but its red-brown color is inconsistent with known Cu-arsenates.

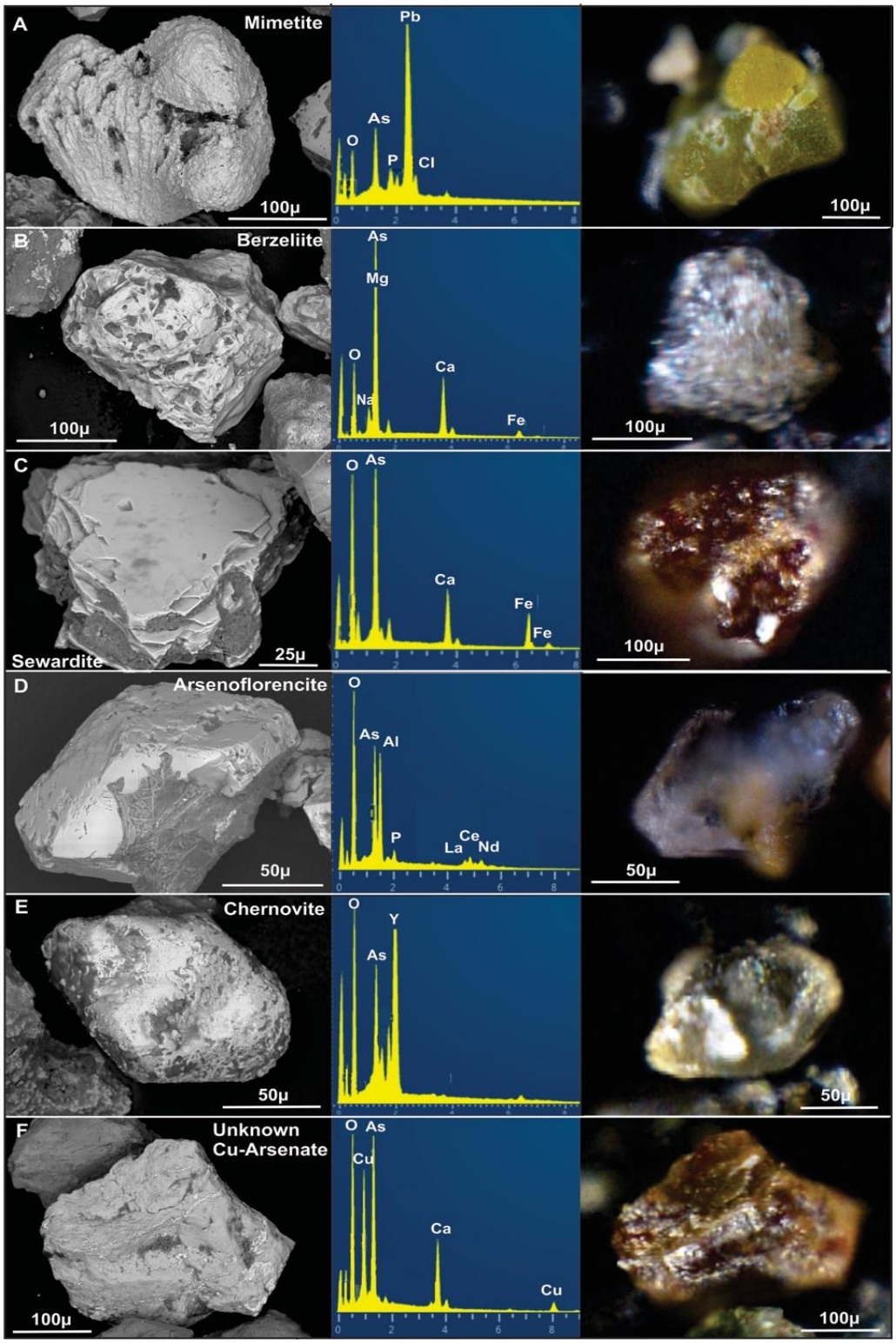

Figure 7. BSE images, EDS spectra, and photograph triplets of arsenates in the heavy mineral concentrate. (**A**) Mimetite; (**B**) Berzeliite; (**C**) Sewardite; (**D**) Arsenoflorencite; (**E**) Chernovite; (**F**) Unknown Cu-Ca arsenate.

Apatite is the most abundant phosphate, but two Pb-bearing phosphates are also present: Clusters of micron-scale crystals of plumbogummite ($PbAl_3(PO_4)(PO_3OH)(OH)_6$) occur embedded in a clay matrix (Figure 8A); yellow, vitreous phosphohedyphane. ($Ca_2Pb_3(PO_4)_3Cl$) occurs as granular masses (Figure 8B). Fluorcalciroméite ($(Ca,Na,\square)_2Sb^{5+}{}_2(O,OH)_6F$ is the only antimonate identified in the Kestel soil. It occurs as honey-yellow, vitreous euhedral crystals with octahedral form (Figure 8C) that in some cases are set in a clay matrix. In addition to calcite and dolomite, the sample contains two other carbonate minerals: Beyerite ($Ca(BiO_2)(CO_3)_2$) was observed as individual anhedral grains (Figure 8D), as well as within composite grains intergrown with clay, cassiterite, and hematite; cerussite ($PbCO_3$) occurs as smooth, rounded grains that are colorless or white (Figure 8E). The colorless Pb-chloride damaraite ($Pb_3O_2(OH)Cl$) forms rounded, anhedral grains with a vitreous luster (Figure 8E).

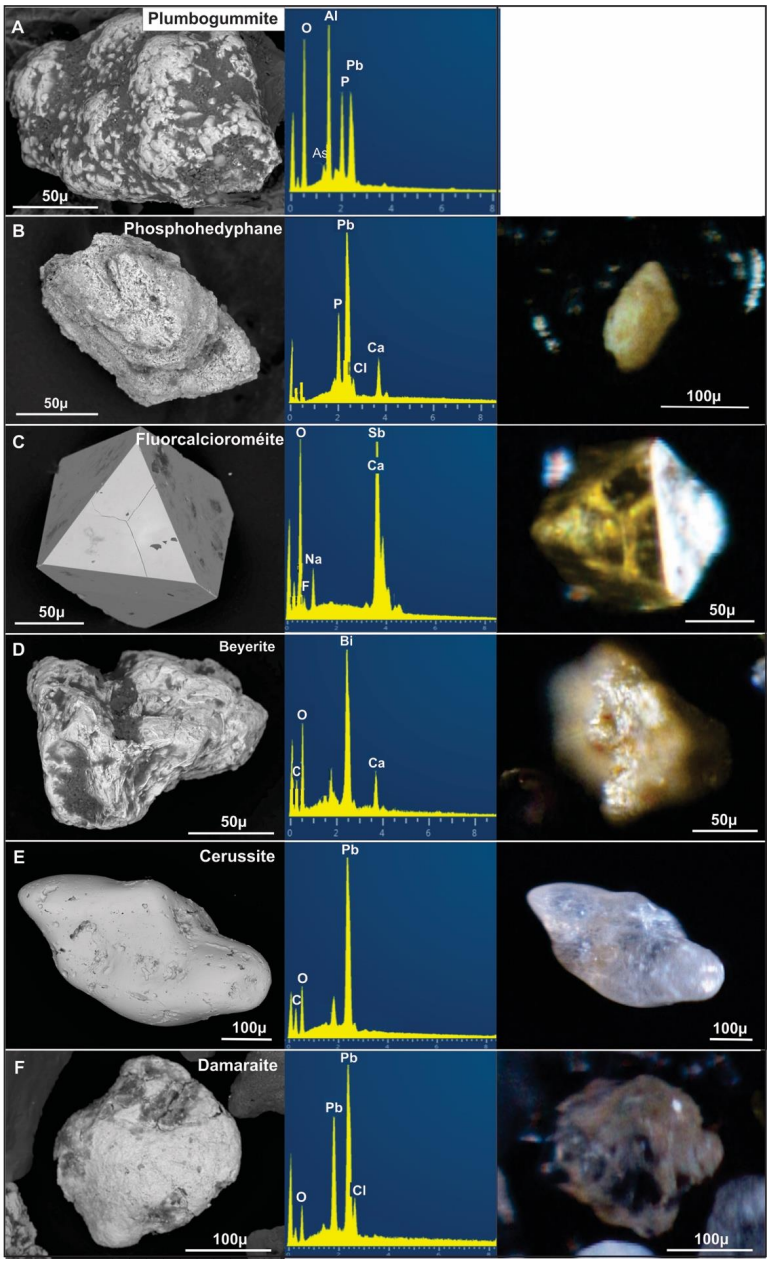

Figure 8. BSE images, EDS spectra, and photograph triplets of carbonates, antimonates, and halides in the heavy mineral concentrate. (**A**) Plumbogummite; (**B**) Phosphohedyphane; (**C**) Fluorcalcioroméite; (**D**) Beyerite; (**E**) Cerussite; (**F**) Damaraite.

The heavy mineral concentrate contains several irregularly shaped, rounded grains composed of very fine-grained intergrowths of Pb, W, and Sb-bearing minerals, including barstowite ($Pb_4Cl_6(CO_3)\cdot H_2O$), raspite ($PbWO_4$), hydrotungstite ($WO_3\cdot H_2O$), and native antimony (Figure 9). In one example, raspite and hydrotungstite encrust the surface of a grain of cerussite (Figure 9E–H), suggesting that these grains are the product of late-stage weathering processes.

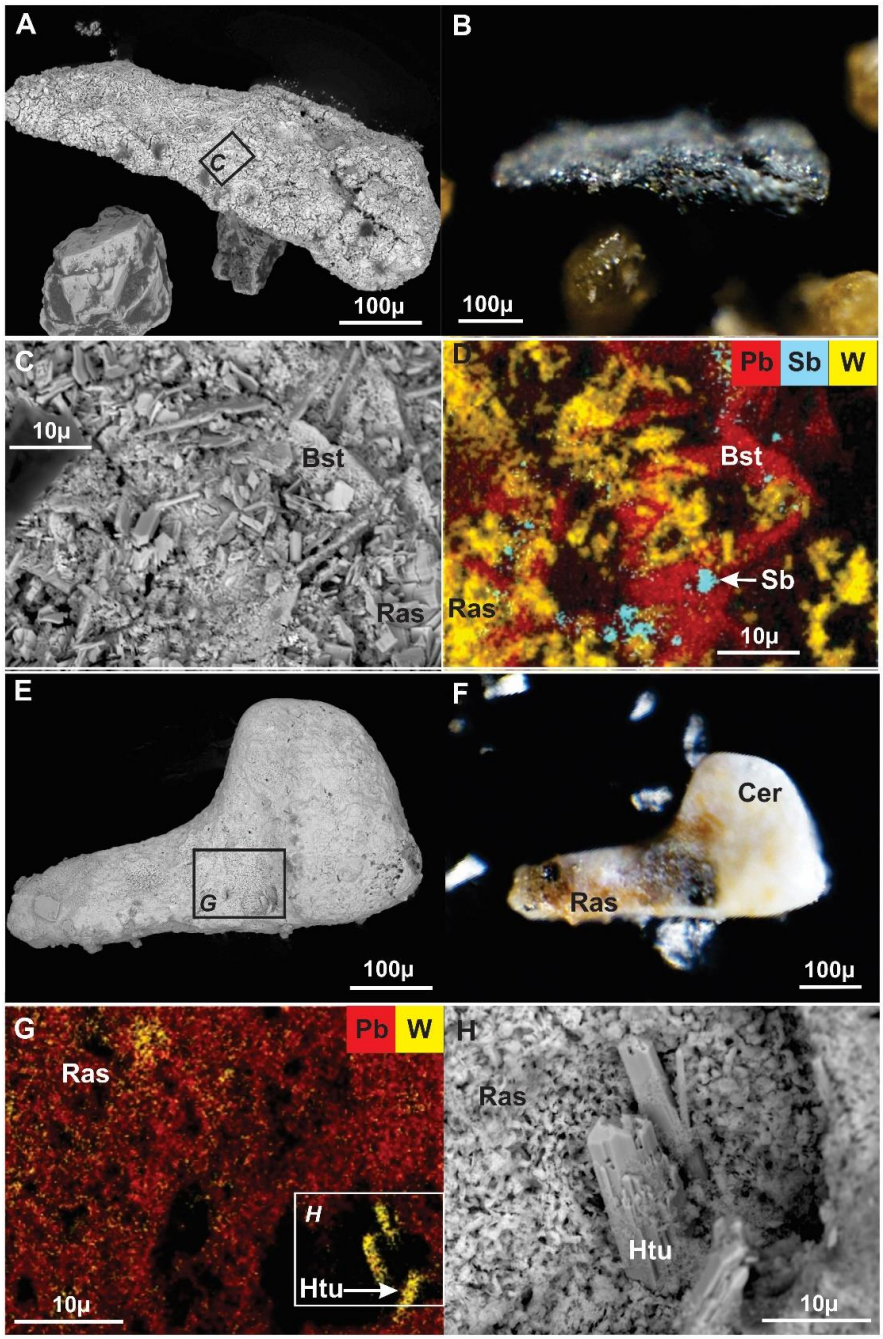

Figure 9. Composite Pb-W-Sb Grains. (**A**) BSE image of fibrous composite grain; (**B**) photograph of Grain (**A**); (**C**) BSE image of close-up on Grain (**A**) showing platy barstowite, bladed respite, and native Sb; (**D**) X-ray map of (**C**); (**E**) BSE image of cerussite grain with raspite on the surface; (**F**) photograph of Grain (**E**); (**G**) X-ray map of closeup of Grain (**E**); (**H**) X-ray map of closeup of image (**G**) showing bladed hydrotungstite. Bst: Barstowite; Sb: Native Antimony; Cer: Cerussite; Ras: Raspite; Htu: Hydrotungstite.

Composite grains that include cassiterite indicate that the original ore was mineralogically more complex than what remains on surface. In addition to assemblages of Cst-Hm-Qtz (Figure 10A), and Cst-Hm-Clay (Figure 10B) that are typical of the remnant mineralization, cassiterite occurs in assemblages with arsenates (sewardite, berzeliite, and a Cu-Ca arsenate) and the Bi-bearing carbonate beyerite (Figure 10C–F), and clay is a common constituent of the matrix of the associated composite grains.

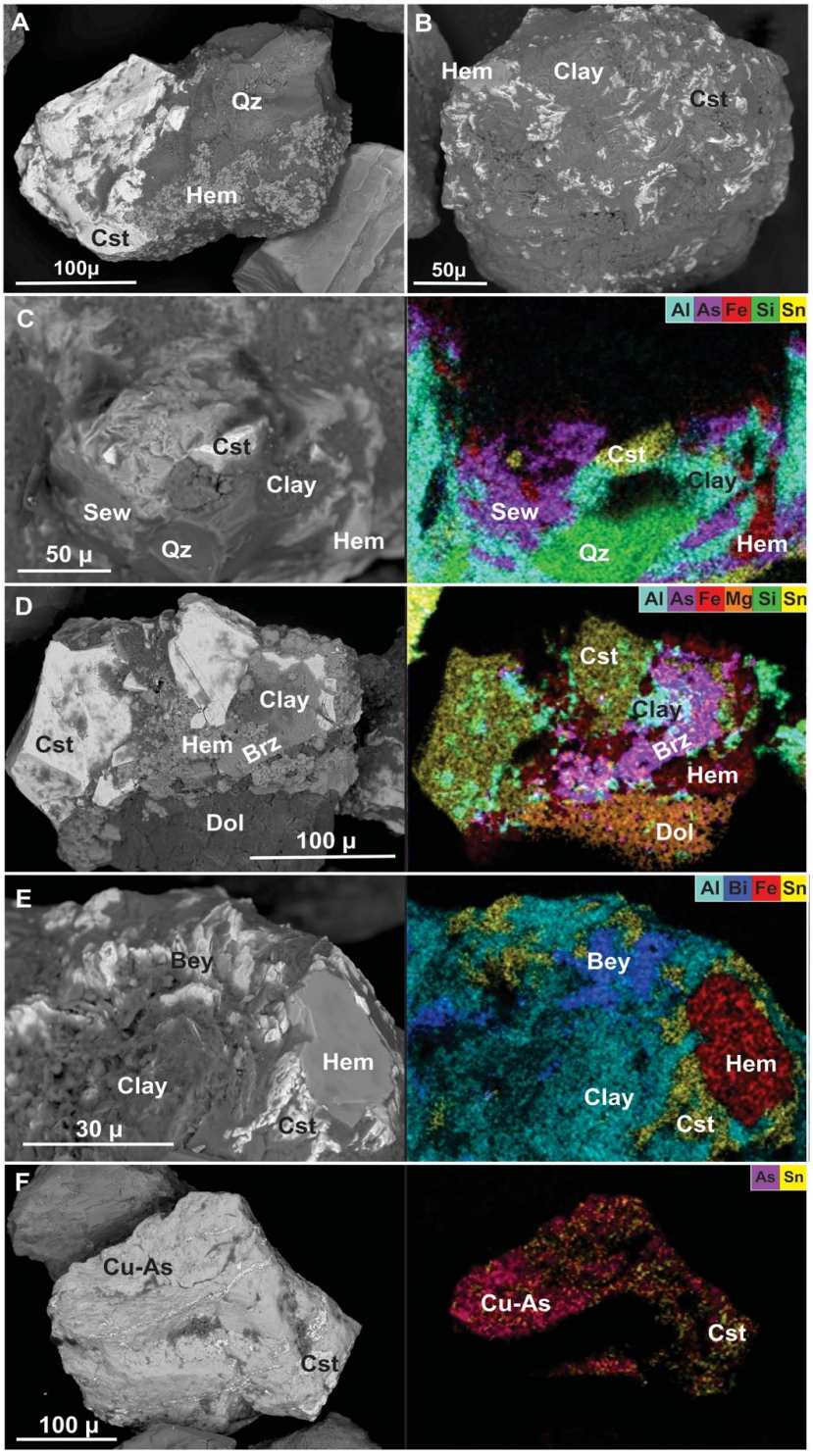

Figure 10. Cassiterite-bearing composite grains. (**A**) Cst-Hem-Qz; (**B**) Cst-Hem-Clay; (**C**) Cst-Hem-Qz-Sew-Clay; (**D**) Cst-Hem-Dol-Brz-Clay; (**E**) Cst-Hem-Bey-Clay; (**F**) Cst-(Cu-Ca Arsenate). Sew: Sewardite; Cst: Cassiterite; Qz: Quartz Brz: Berzeliite; Dol: Dolomite; Bey: Beyerite.

4. Discussion

Examination of the hematite-rich material remaining as outcropping veins and as loose material on the surrounding hillside confirms the findings of Çağatay and Pehlivan [27] that this material is mineralogically simple, consisting primarily of hematite, quartz, carbonate minerals, and minor cassiterite. However, the ore is highly variable on a centimeter scale with cassiterite concentrated in late fractures and breccia matrix. Within a single hand sample, pXRF spot analyses for Sn varied from undetectable to 4%.

One previously undocumented feature of the ores is the association of clay with cassiterite-bearing assemblages in both surface samples and composite grains in the soil of the Kestel mine. The presence of clay in ore assemblages has implications for ore dressing. A clay-rich matric would be easier to crush, and facilitate the separation of ore minerals from the matrix.

Other than hematite and cassiterite, Çağatay and Pehlivan [27] documented few ore minerals: Chalcocite, arsenopyrite, native bismuth, and gold; rutile and titanite were present, but were interpreted to have been sourced from the local gneisses. The presence of gold and arsenopyrite were confirmed by Muhly et al. [13]. These compositionally simple assemblages lie in sharp contrast to the diversity of minerals and heavy metal elements found within the soil inside the mine. A total of 27 heavy metal-bearing minerals were identified in the heavy mineral concentrate, including minerals containing Ti, Cr, Fe, Cu, As, Y, Sn, Sb, La, Ce, Nd, W, Au, Hg, Pb, and Bi.

Most of the ore minerals occur as phosphates, arsenates, carbonates, antimonates, and tungstates. No such minerals have been found in surface finds. Based on their textures it is likely that some of these minerals (native antimony, barstowite, hydrotungstite, phosphohedyphane, raspite) formed during post-depositional weathering processes. However, many of the remaining minerals display euhedral to subhedral forms, and can be found in assemblages intergrown with cassiterite, hematite, dolomite, and clay within composite grains. Thus, they appear to be primary components of the ore.

Only a single grain of gold was found in the mine soil sample, indicating that although present, gold was not a major component of the extracted ore. Based on descriptive criteria outlined by Williams et al. [28], Kestel is clearly not an IOCG deposit: It lacks copper mineralization and pervasive alkali metasomatism, as well as many components of the distinct set of IOGC-associated elements (F, Co, Ni, Mo, Ag, U). Cassiterite is the only non-ferrous ore mineral that is present at <0.1%, and so was the most likely mineral that was extracted in the Early Bronze Age at Kestel, as was initially suggested by Yener et al. [5]. It would seem to be a variant of the iron mineralization that is common in the Niğde Massif, rather than an example of IOGC ore.

The contrast between the elemental and mineralogical composition of detritus within the mine compared to the surface exposures and waste rock demonstrates that the extracted ore was significantly different in composition and character from the remaining cassiterite-bearing hematite-quartz veins. Given that such exposed veins were left unmined attests to them having been recognized as waste by the prehistoric miners. Accordingly, the grade and character of the existing veins cannot be used to extrapolate the quality, composition, or physical properties of the ore that was mined.

Interestingly, the association of cassiterite and hematite with an arsenate (yazganite, $NaFe_2^{3+}(Mg,Mn)(AsO_4)_3 \cdot H_2O$) has been documented at Hisarcik, near Kayseri, approximately 60 km to the northeast (Yazgan, 2005). In this case, the ore occurs as coatings on near-surface extension veins in andesitic pyroclastic rocks of the Erciyes volcanic complex and are interpreted to have formed through condensation in a fumarole [29,30]. Many of these veins are found in ancient mining galleries that can be dated to the Early Bronze Age by associated pottery [6]. Thus, this unusual form of tin-arsenate mineralization must have contributed to the development of the bronze economy of Central Anatolia, if not beyond, and may account for common ternary bronzes (Cu-Sn-As) in some of the earliest bronze artifacts of the region.

5. Conclusions

1. Remnant exposures of Kestel mineralization are composed of mineralogically simple assemblages (Hem + Qz ± Cst ± Tur ± Cal ± Clay) with trace Apy, Bi, and Au.
2. The heavy mineral assemblage preserved in sediments within the mine are far more complex than that of surface veins, with 27 heavy-metal bearing minerals identified, and the additional elemental components Sb, REEs, W, Hg, and Pb. Thus, the remnant mineralization is not representative of the ore that was extracted.
3. Arsenates are the most diverse group of minerals within heavy mineral fraction, and they are directly associated with cassiterite.
4. The scarcity of Cu, Au, and the lack of elements including Co, Ni, U, and F indicate that Kestel is not an OICG deposit. Rather the shallowly emplaced Hem + Qz + Cst + Arsenates ores appear to be a regional feature, occurring both at Kestel and at Hisarcık, and so may represent a new target for tin exploration in Central Turkey.
5. With cassiterite being the only non-ferrous ore mineral present at <1%, and the paucity of gold both in mine sediments and surface veins it is clear that Kestel was a large-scale tin mine in the Early Bronze Age.
6. Activities at Kestel represent the earliest evidence thus far for an emerging pattern of local tin exploitation that may continue into the Late Bronze Age. More definitively, this evidence demonstrates that Central Turkey was a significant tin producer in the Early Bronze Age, a millennium before nearby Kültepe-Kanesh arose as an administrative trade center that is known to have imported tin from Central Asia.

Author Contributions: Contributions were made to this paper as follows: Conceptualization, W.P., E.Y., and M.J.; methodology, W.P. and M.J.; formal analysis, W.P.; resources, K.A.Y. and R.M.; data curation, W.P.; writing—original draft preparation, W.P.; writing—review and editing, W.P., E.Y., M.J., K.A.Y., and R.M.; visualization, W.P.; funding acquisition, W.P., M.J., and K.A.Y. All authors have read and agreed to the published version of the manuscript.

Funding: This research was funded by PSC-CUNY Grant 62609-00 50, The Tow Faculty Research Travel Fellowship, and the University of Chicago Helen Rich Travel and Research Grant, and the Fund for Amuq Valley Archaeological Expeditions (FAVAE) Grant # 26-0531114.

Data Availability Statement: The data presented in this study are available on request from the corresponding author.

Acknowledgments: The authors wish to thank Fazıl Açıkgöz, Director of the Niğde Archaeological Museum, and Esat Esen, the watchman of the Göltepe depot, for their advice and assistance.

Conflicts of Interest: The authors declare no conflict of interest.

References

1. Muhly, J. Sources of tin and the beginnings of bronze metallurgy. *Am. J. Arch.* **1985**, *89*, 275–291. [CrossRef]
2. Penhallurick, R. *Tin in Antiquity*; The Institute of Metals: London, UK, 1986; 271p.
3. Garner, J. Bronze Age tin mines in central Asia. In *Archaeometallurgy in Europe III*; Hauptmann, A., Modarressi-Tehrani, D., Eds.; Deutsches Bergbau-Museum: Bochum, Germany, 2015; pp. 135–143.
4. Berger, D.; Soles, J.S.; Giumlia-Mair, A.R.; Brügmann, G.; Galili, E.; Lockhoff, N.; Pernicka, E. Isotope systematics and chemical composition of tin ingots from Mochlos (Crete) and other Late Bronze Age sites in the eastern Mediterranean Sea: An ultimate key to tin provenance? *PLoS ONE* **2019**, *14*, e0218326. [CrossRef] [PubMed]
5. Yener, K.A.; Özbal, H.; Kaptan, E.; Pehlivan, A.N.; Goodway, M. Kestel: An Early Bronze Age source of tin ore in the Taurus Mountains, Turkey. *Science* **1989**, *244*, 200–203. [CrossRef] [PubMed]
6. Yener, K.A.; Kulakoğlu, F.; Yazgan, E.; Kontani, R.; Hayakawa, Y.; Lehner, J.; Dardeniz, G.; Öztürk, G.; Johnson, M.; Kaptan, E.; et al. New tin mines and production sites near Kultepe in Turkey: A third-millennium BC highland production model. *Antiquity* **2015**, *345*, 596–612. [CrossRef]
7. Durman, A. Tin in southeastern Europe? *Opusc. Archaeol.* **1997**, *21*, 7–14.
8. Mason, A.; Powell, W.; Bankoff, H.A.; Mathur, R.; Price, M.; Bulatović, A.; Filipović, V. Provenance of tin in the Late Bronze Age Balkans based on probabilistic and spatial analysis of Sn isotopes. *J. Arch. Sci.* **2020**, *122*, 105181. [CrossRef]

9. Yener, K.A. Revisiting Kestel Mine and Göltepe: The dynamics of local provisioning of tin during the Early Bronze Age. In *Ancient Mining in Turkey and the Eastern Mediterranean*; Yalçın, Ü., Özbal, H., Paşamehmetoğlu, A.G., Eds.; Atılım University: Ankara, Turkey, 2008; pp. 57–64.
10. Yener, K.A.; Vandiver, P. Tin processing at Göltepe, an Early Bronze Age site in Anatolia. *Am. J. Arch.* **1993**, *97*, 207–238. [CrossRef]
11. Earl, B.; Özbal, H. Early Bronze Age tin processing at Kestel/Göltepe, Anatolia. *Archaeometry* **1996**, *38*, 289–303. [CrossRef]
12. Öztürk, H.; Hanlinçi, N. Metallogenic evaluation of Turkey: Implications for tin sources of Bronze Age in Turkey. *Tuba-Ar-Turk. Acad. Sci. J. Archaeol.* **2009**, *12*, 105–116.
13. Muhly, J.; Begemann, F.; Öztunali, Ö.; Pernicka, E.; Schmitt-Strecker, S.; Wagner, G. The bronze metallurgy of Anatolia and the question of local tin sources. *Archaeometry* **1991**, *90*, 209–220.
14. Whitney, D.; Teyssier, C.; Heizler, M. Gneiss domes, metamorphic core complexes, and wrench zones: Thermal and structural evolution of the Niğde Massif, central Anatolia. *Tectonics* **2007**, *28*, TC5002. [CrossRef]
15. Hall, M.; Steadman, S. Tin and Anatolia-Another Look. *J. Mediterr. Arch.* **1991**, *4*, 217–234. [CrossRef]
16. Pernicka, E.; Wagner, G.; Muhly, J.; Öztunali, Ö. Comment on the discussion of ancient tin sources in Anatolia. *J. Mediterr. Arch.* **1993**, *5*, 91–98. [CrossRef]
17. Muhly, J. Early Bronze Age tin and the Taurus. *Am. J. Arch.* **1993**, *97*, 239–253. [CrossRef]
18. Yigit, O. Gold in Turkey—A missing link in Tethyan metallogeny. *Ore Geol. Rev.* **2006**, *28*, 147–179. [CrossRef]
19. Kuşcu, I.; Yılmazer, E.; Güleç, N.; Bayır, S.; Demilela, G.; Kuşcu, G.; Kuru, G.; Kaymakçı, N. U-Pb and ^{40}Ar-^{39}Ar geochronology and isotopic constraints on the genesis of copper-gold-bearing iron oxide deposits in the Hasançelebi district, Eastern Turkey. *Econ. Geol.* **2011**, *106*, 261–288.
20. Yılmazer, E.; Güleç, N.; Kusçu, I.; Lentz, D. Geology, geochemistry, and geochronology of Fe-oxide CU (±Au) mineralization associated with Şamlı pluton, western Turkey. *Ore Geol. Rev.* **2014**, *57*, 191–215. [CrossRef]
21. Yener, K.A. *The Domestication of Metals: The Rise of Complex Metal Industries in Anatolia*; Brill: Leiden, The Netherlands; Boston, MA, USA; Koln, Germany, 2000; 228p.
22. Whitney, D.; Teyssier, C.; Fayon, A.; Hamilton, M.; Heizler, M. Tectonic controls on metamorphism, partial melting, and intrusion: Timing and duration of regional metamorphism and magmatism in the Niğde Massif, Turkey. *Tectonophysics* **2003**, *376*, 37–60. [CrossRef]
23. Kurt, H.; Koçak, K.; Asan, K.; Karakaş, M. Petrogenesis of the Üçkapılı granitoid and its mafic enclaves in Elmalı area (Niğde, Central Anatolia, Turkey. *Acta Geol. Sin.* **2013**, *87*, 738–748. [CrossRef]
24. Kuşcu, I. Skarns and skarn deposits of Turkey. In *Mineral Resources of Turkey*; Pirajno, F., Ünlü, T., Dönmez, C., Şahin, M.B., Eds.; Springer Nature: Cham, Switzerland, 2019; pp. 283–336.
25. Tumuklu, A.; Altuncu, S.; Ozgur, F. Mineralogy of the iron mineralizations associated with the Uckapili granitoid (Nigde Massif). *Int. J. Eng. Res. Man* **2016**, *3*, 2058–2349.
26. Akçay, M. Geological and mineralogical investigation of the Gümüşler (Niğde) Sb±Hg±W occurrences and implications on their gold potential. *Geol. Bul. Tur.* **1995**, *38*, 11–22.
27. Çağatay, A.; Pehlivan, N. Mineralogy of the Celaller (Niğde-Çamardi) tin mineralization. *Geol. Eng.* **1988**, *32–33*, 27–31.
28. Williams, P.J.; Barton, M.D.; Johnson, D.A.; Fontboté, L.; De Haller, A.; Mark, G.; Oliver, N.H.S.; Marschik, R. Iron Oxide Copper-Gold Deposits: Geology, Space-Time Distribution, and Possible Modes of Origin. In *Economic Geology*; 100th Anniversary Volume; Society of Economic Geologists: Lyttelton, CO, USA, 2005; pp. 371–405.
29. Yazgan, E. Cassiterite (tin) mineralization related with Erciyes volcanic activities and the mode of formation of the magnetite-cassiterite-yazganite-tridymite paragenesis. In Proceedings of the 58th Geological Congress of Turkey Abstracts, Ankara, Turkey, 11–17 April 2005; pp. 135–138.
30. Yazgan, E. Erciyes volcanic activities and the mode of formation of the hematite-cassiterite-yazganite-tridymite paragenesis and its implication for bronze alloys. In Proceedings of the 1st Kültepe International Meeting, Studies Dedicated to Kutlu Emre, Kültepe, Turkey, 19–23 September 2013; Kulakoğlu, F., Michel, C., Eds.; pp. 183–194.